General Disclaimer

One or more of the Following Statements may affect this Document

- This document has been reproduced from the best copy furnished by the organizational source. It is being released in the interest of making available as much information as possible.

- This document may contain data, which exceeds the sheet parameters. It was furnished in this condition by the organizational source and is the best copy available.

- This document may contain tone-on-tone or color graphs, charts and/or pictures, which have been reproduced in black and white.

- This document is paginated as submitted by the original source.

- Portions of this document are not fully legible due to the historical nature of some of the material. However, it is the best reproduction available from the original submission.

Solid/Melt Interface Studies of High-Speed Silicon Sheet Growth

Quarterly Technical Progress Report 1

T. F. Ciszek

SERI

Solar Energy Research Institute

A Division of Midwest Research Institute

1617 Cole Boulevard
Golden, Colorado 80401

SERI/PR-212-2196

SOLID/MELT INTERFACE STUDIES OF HIGH-SPEED SILICON SHEET GROWTH

Quarterly Technical Progress Report 1
July 15, 1983 - October 15, 1983

T. F. Ciszek
Principal Investigator

Solar Energy Research Institute
Solid State Research Branch
Golden, CO   80401

February 1984

Prepared for the
Flat Plate Solar Array Project

TABLE OF CONTENTS

LIST OF FIGURES

1. SUMMARY

Radial growth-rate anisotropies and limiting growth forms of point-nucleated, dislocation-free silicon sheets spreading horizontally on the free surface of a silicon melt have been measured for (100), (110), (111), and (112) sheet planes. Sixteen-millimeter movie photography was used to record the growth process. Analysis of the sheet edges has lead to predicted geometries for the tip shape of unidirectional, dislocation-free, horizontally growing sheets propagating in various directions within the above-mentioned planes. Similar techniques were used to study polycrystalline sheets and dendrite propagation. For dendrites, growth rates on the order of 2.5 m/min and growth rate anisotropies on the order of 25 were measured.

1

2. INTRODUCTION

This work investigates the growth kinetics and growth forms of silicon sheet crystals nucleated at a small diameter and allowed to spread radially outward in all directions on a supercooled horizontal silicon melt surface. Generally, the crystal faces that grow most slowly are those with the closest packing. As pointed out by Jackson [1], these should also be the faces with the lowest specific surface free energy. Thus, there is reason to expect that the equilibrium form and the observed macroscopic growth form will be similar. In fact, attempts have been made to predict the low surface free energy faces from calculations of the reticular density of atoms in a plane [2,3].

Equilibrium forms are governed by the variation of surface free energy with crystal orientation as described by the classic work of Wulff [4]. Further amplification of Wulff's concepts was provided by Herring [5]. In these treatments, a polar plot of specific surface free energy versus crystal orientation (called a Wulff plot) is constructed. The distance from the origin in a particular direction is proportional to the surface free energy for the crystal orientation corresponding to that direction. In general, the plot is a three-dimensional closed surface with a number of minima and maxima. If planes perpendicular to the radius vector are imagined at each point on the closed surface, then the volume that can be reached from the origin without crossing any planes defines the equilibrium shape or form of the crystal. Since sharp minima or cusps in the polar plot have the shortest radius vectors, planes normal to the radius at these cusp positions will dominate the equilibrium shape.

Sheet crystals are approximately two-dimensional; hence, a planar section through the Wulff plot coincident with the sheet surface plane is useful in describing the equilibrium shape. Detailed data for the variation of surface free energy with orientation is not available for silicon. However, it is generally acknowledged that the (111) planes have the lowest surface free energy, and vestiges of these planes are responsible for the observable "growth lines" on crystals constrained to grow in a cylindrical ingot form. As mentioned earlier, the value of the surface free energy for a particular crystal plane is a function of the free bond density. This is lowest for (111) planes.

Observations of (100), (110), (111), (112), and polycrystalline sheets propagating radially from small-diameter sources on a free melt surface were made by 16-mm photography. Dendrite propagation was also recorded in this manner. From the films and post-growth examination of the crystals, it was possible to deduce the idealized equilibrium polygonal shapes of the sheets. On the hypothesis that growth forms and equilibrium forms are similar for these sheets, qualitative Wulff plots that locate the cusp minima in the various sheet planes were constructed. In addition, information about growth rate anisotropies in the sheet planes has been obtained. From the geometry of the sheet edges, it is possible to determine the criteria that govern the tip-shape of single-crystal silicon sheets growing horizontally from a melt surface.

2

3. EXPERIMENTAL PROCEDURE

Silicon was melted in a quartz crucible 60 mm in diameter and 25 mm high. Induction heating with a graphite susceptor was used. The susceptor was insulated by a cylindrical opaque quartz tube with a 6-mm wall thickness. An inert atmosphere of argon was maintained in the 400-mm-diameter by 1500-mm-high growth chamber. The top of the chamber was fitted with a gate valve that allowed reseeding from a second chamber above the first. Thus, all sheet propagation studies could be done from the same melt. Sheet growth was initiated by dipping a seed crystal of the desired orientation into the melt and growing a thin neck from the seed at 15 rpm rotation rate in order to produce a dislocation-free, small (0.5 to 1.5 mm in diameter) cylindrical crystal. A sheet was then allowed to propagate radially in all directions on the melt surface by setting the vertical pulling speed to zero, dropping the RF generator power level to 94.7% of the value at which the neck was grown, and lowering the rotation rate to 1 rpm. A slow rate was used to avoid imposing a round shape on the spreading sheet. However, a nonzero rate was needed to allow measurements of all crystal faces on movie films of the growth. For each seed orientation, a second sheet was grown from a larger diameter (3.8 to 6.2 mm), dislocation-free, round cylindrical starting condition. Since the transformation from round to equilibrium shape occurs in a distance which is a function of initial round diameter, this allowed viewing the transformation on two different size scales.

The sheets did not grow perfectly flat and tended to have a slightly convex bottom since some growth occurred downward into the melt while the sheets were spreading radially. The radial growth rate of the sheets as they approached their equilibrium shapes was typically in the range of from 7 to 15 mm/min for the 5.3% power reductions used in these studies. At some point in the growth, icing from the crucible walls moved radially inward to close proximity with the spreading sheets. The sheets were removed from the melt at this time by quickly pulling the seed upward. The observations of dendrite propagation were made by nucleating dendrites at the crucible walls as large reductions (30%-40%) were made in the RF generator power.

Records of the sheet and dendrite growth experiments were made with 16-mm movie photography. The camera was located outside a window of the growth chamber and a polished silicon mirror was used to direct light rays from the growth area to the camera, as shown in Figure 1. A filming speed of 10 frames/s was used in the sheet growth studies. The typical growth duration was 140 seconds, and since a rotation rate of 1 rpm was used, the crystal revolved just over two times during the filming. This allowed any particular diameter of the growing sheet to be measured 5 times. Measurements were made of the distance between parallel flat faces and of the diameters of the faster growing diagonally opposed regions located angularly between two successive flat faces. Figure 2 is the view the camera sees. In this case, a (110) sheet growing at its equilibrium shape is shown. The measurements were made from the film by passing it under a low-power (8-40X) microscope with a reticle placed over the film. A 50-frames/s filming rate was used for the dendrite studies, since the growth rate was much faster than for sheets.
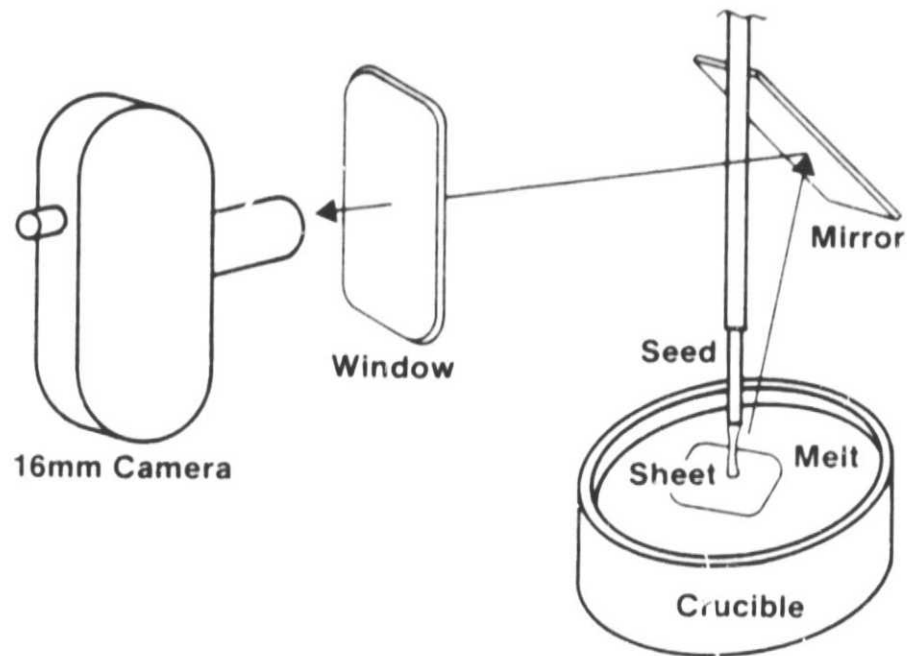
Figure 1. Schematic of arrangement used to film radially growing sheets
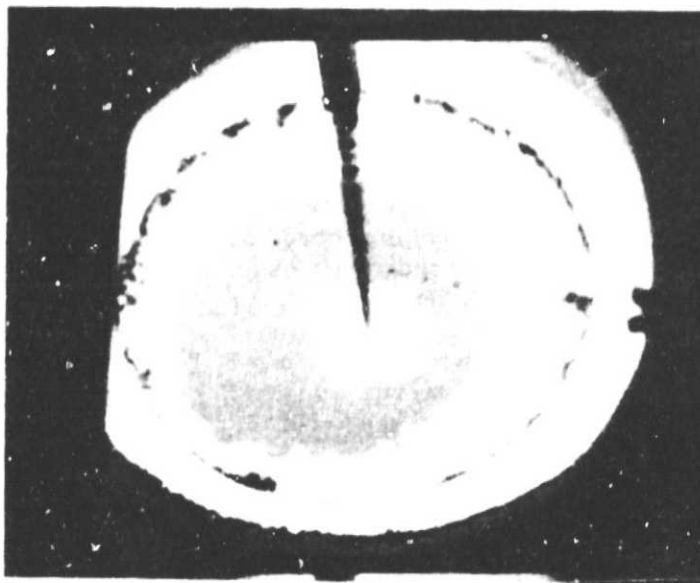

Figure 2. One 16-mm frame from a film showing the limiting growth shape of a (110) sheet

4. RESULTS AND DISCUSSION

4.1 Equilibrium Sheet Shapes

The equilibrium shape of a (100) dislocation-free silicon sheet is a square. Figure 3a shows this form for a sheet grown from a 1.2-mm-diameter, round starting shape. The transformation to the square shape occurs in about 3-4 seed diameters; thus, the sheet is square at a small size. The idealized square shape is shown in Figure 3b. The edges are in the four <011> directions, and the corners lie along the four <001> directions. The Wulff plot in the (100) plane is expected to have minima at the four (011) planes normal to the sheet surface and larger values in other directions. This is qualitatively shown by the curved, four-lobed figure surrounding the equilibrium shape.

Sheets nucleated in the (111) plane transform from a round shape to hexagonal with equal 120 degree angles (Figure 4a). The sides of the hexagonal shape are in <$\bar{1}\bar{1}2$> radial directions, while the corners are in <$\bar{1}10$> directions. The hypothetical Wulff plot is drawn with six cusps on the ($\bar{1}\bar{1}2$) planes bounding the idealized sheet shape shown in Figure 4b.

At first glance, the growth form of (110) sheets also appears to be a regular hexagon (Figure 5a). However, closer examination shows that there is less symmetry in the (110) shape. Four of the six polygonal sides lie in <$\bar{1}11$> directions and the angle between two such adjacent sides is only 109.471 degrees as shown in Figure 5b. The corners between two such sides lie in [$\bar{1}10$] and [1$\bar{1}0$] directions. Two sides of the polygonal shape are opposite each other and in the [001] and [00$\bar{1}$] directions. These sides make an angle of 125.264 degrees with the ($\bar{1}11$) type sides. Minima occur both on (001) type planes and on ($\bar{1}11$) type planes in the qualitative Wulff plot.

The (112) plane sheets are observed to also have six sides, as can be seen in the sheet crystal of Figure 6a. However, the bounding faces and included angles are different from both the (111) and (110) sheet cases. Two opposite sides are in <$\bar{1}\bar{1}1$> directions. The other four sides correspond to predicted Wulff plot cusps on ($2\bar{4}1$) type planes. Two adjacent sides of this type make an angle of 135.585 degrees with each other. The corners between these sides are in [$\bar{1}10$] and [1$\bar{1}0$] directions. The angle between ($2\bar{4}1$) and ($\bar{1}\bar{1}1$) type sides is 112.208 degrees. The deduced Wulff plot shows minima on both ($\bar{1}\bar{1}1$) and ($2\bar{4}1$) type planes (Figure 6b).

The Wulff plots in Figures 3 through 6 are only hypothetical. It is reasonably certain that minima occur where they are shown. Whether the minima are sharp cusps or only shallow valleys is not known. There is more uncertainty about the nonminima portions of the plots. Thus, they are shown as dotted lines in the figures. Angles observed on the sheet crystals agree very well with the angles on the idealized growth shapes in the figures. Since no special effort was made to reduce thermal asymmetry in the hot zone, the sheet crystal forms were sometimes asymmetrical. That is, the distance from the seed to two equivalent flat edges was not always equal.
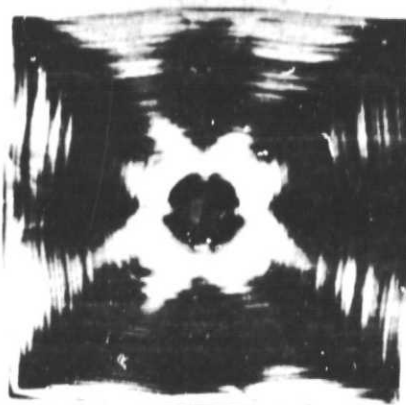
Figure 3a. Final shape of a (100) sheet

Figure 3b. Idealized equilibrium form and qualitative Wulff plot
for a (100) sheet
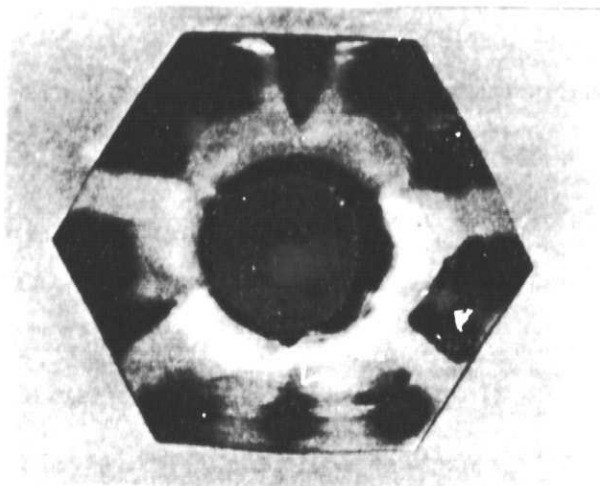
Figure 4a. Final shape of a (111) sheet

(111) PLANE

Figure 4b. Idealized equilibrium form and qualitative
Wulff plot for a (111) sheet
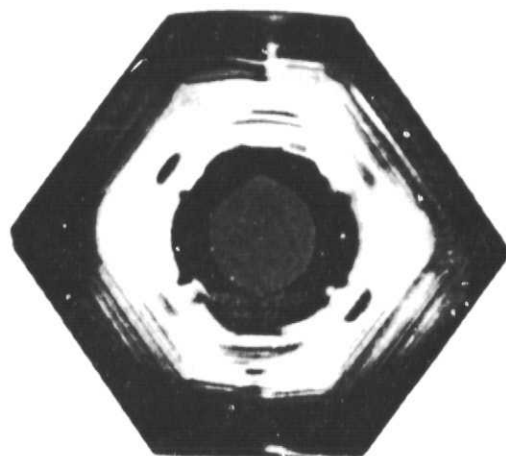
Figure 5a. Final shape of a (110) sheet

(110) PLANE

Figure 5b. Idealized equilibruim form and qualitative
Wulff plot for a (110) sheet

8

Figure 6a. Final shape of a (112) sheet

$\bar{1}\bar{1}1$ 112.2°

$\bar{2}4\bar{1}$ $4\bar{2}\bar{1}$

135.6° $\bar{1}10$

$4\bar{2}\bar{1}$ $\bar{2}4\bar{1}$

$11\bar{1}$

(112) PLANE
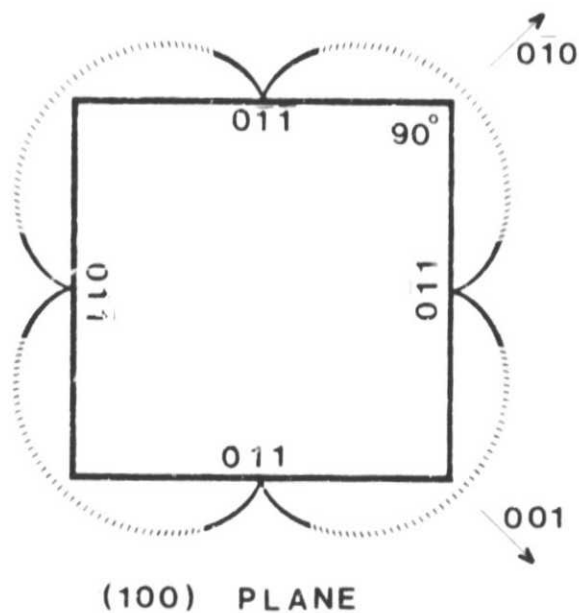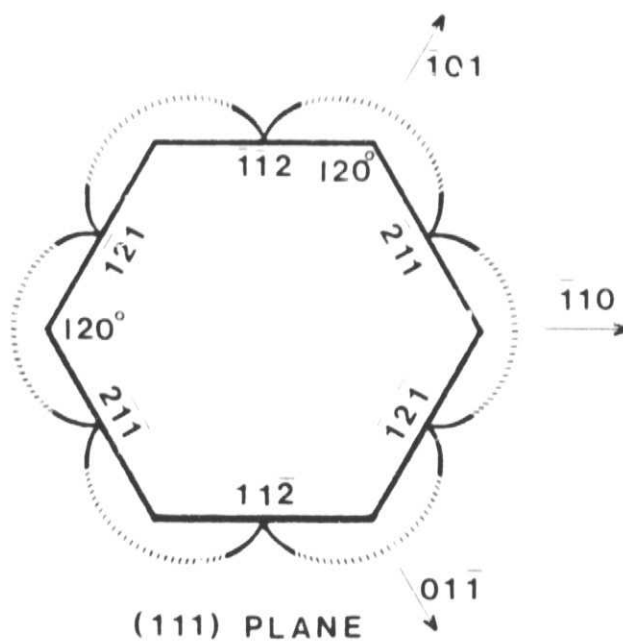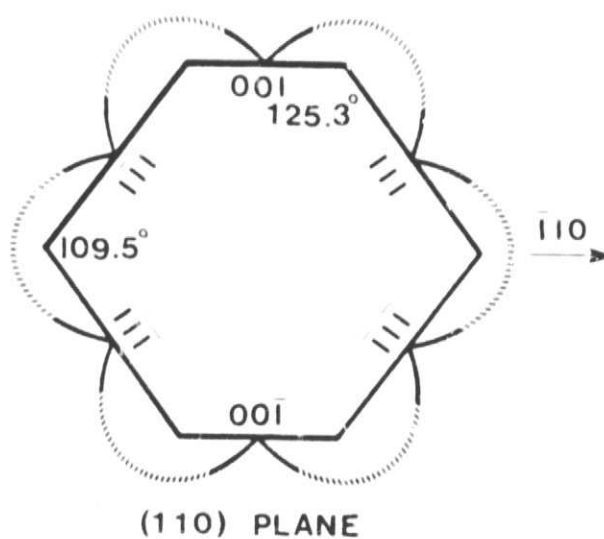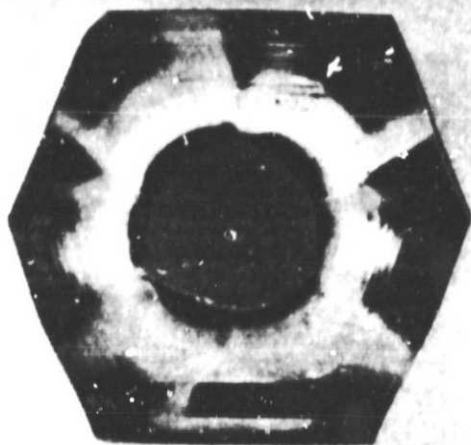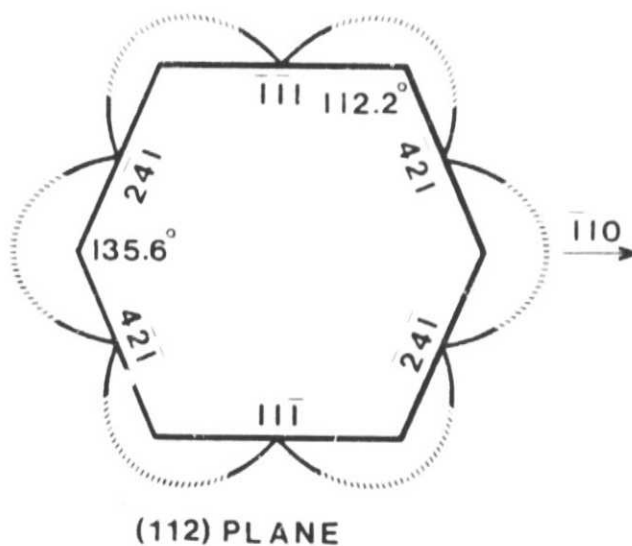
Figure 6b. Idealized equilibrium form and qualitative
Wulff plot for a (112) sheet

9

4.2 Sheet Edge Geometries

A strong (111) faceting effect was observed on the edge regions of the sheets largely because dislocation-free growth was employed for the sheet experiments. In the absence of dislocations, nucleation of new growth is more difficult and larger levels of supercooling arise at the leading edges of the growth front. Faceting accompanies this situation. One (100) sheet was grown from a dislocated starting configuration. Two effects were noted with this sheet. The edge faceting was much less pronounced and in fact was nearly absent. Also, the idealized square shape did not completely form, at least not in the growth times available in our experimental set-up. The corners of the sheet remained well-rounded.

The edge faceting in dislocation-free sheets always appeared on (111) planes. An example is depicted in the photograph of Figure 7, which shows a (111) sheet mounted in wax to allow viewing of the edge. The central edge facet in the photograph makes a 70.5-degree acute angle with the top of the sheet. It is located in a $\langle 2\bar{1}\bar{1} \rangle$ type direction from the seed. To the left and right of this facet are other edge facets that make a 109.5-degree obtuse angle with the sheet's top surface. These are in $\langle \bar{2}11 \rangle$ directions from the seed. All told, there are three obtuse facets and three acute facets alternating around the sheet edge. Careful scrutiny of Figure 7 also reveals a (111) facet on the sheet top adjacent to the central edge facet. There are six of these, one adjacent to each edge facet.

These observations have implications for high-perfection sheet growth solid/liquid interfaces, both in vertical and horizontal modes. It is possible to predict, for example, the sheet tip geometries for a large number of growth orientations from the observations on radially spreading sheets. I have done this for the horizontal, large-area solid/liquid interface growth geometry. Figure 8 shows the expected tip geometries for (111) dislocation-free sheets growing in the $\langle 2\bar{1}\bar{1} \rangle$ and $\langle \bar{2}11 \rangle$ type directions, with a 5-degree pulling angle. Note the retrograde tip angle for $\langle \bar{2}11 \rangle$ growth.

For (100) sheets, four (111) edge facets appear in $\langle 011 \rangle$ directions from the seed. All make 54.7-degree acute angles with the top of the sheet. The expected tip geometry for dislocation-free (100) silicon sheets growing in one of these four directions is given in Figure 9.

The edges of (110) sheets displayed two types of (111) facets. In the four $\langle 1\bar{1}\bar{1} \rangle$ type directions, a 90-degree facet with respect to the sheet plane was found. In the two $\langle 001 \rangle$ directions, the facet made a 35.3-degree acute angle with the sheet top. The 144.7-degree obtuse (111) facets were not observed. Predicted sheet tip geometries for horizontal growth are drawn in Figure 10.

The greatest variety of edge facets was seen in (112) sheets. Figure 11 shows these in the way they would define the tip geometries of horizontal sheets. In the [11$\bar{1}$] direction, a facet at 90 degrees to the sheet plane was seen, while in the [$\bar{1}\bar{1}$1] direction, two facets appeared. One was at 90 degrees to the sheet plane and a second was at 19.5 degrees. Figure 12 is a photograph of a portion of the underside of a (112) sheet showing the large-area 19.5-degree facet. The ($\bar{1}\bar{1}$1) edge of the sheet is at the top in the photograph, and the facet at this edge is also discernable in the photograph.

10
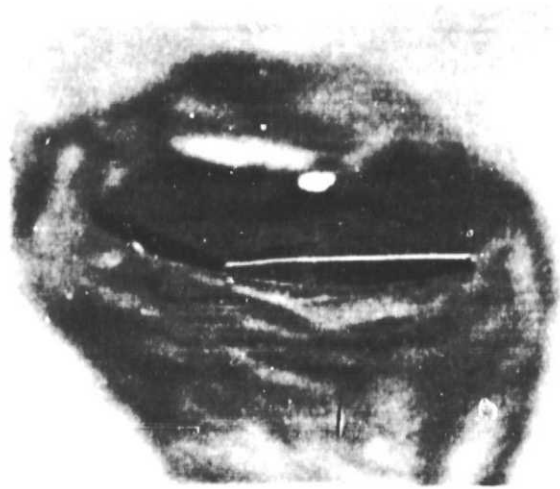
Figure 7. Edge facets on a (111) dislocation-free sheet mounted in wax

(111) SHEET

$[2\bar{1}\bar{1}]$

5°   70.5° $(1\bar{1}\bar{1})$
          SOLID   MELT

(111) SHEET

$[\bar{2}11]$

5°   109.5° $(1\bar{1}1)$
          SOLID   MELT
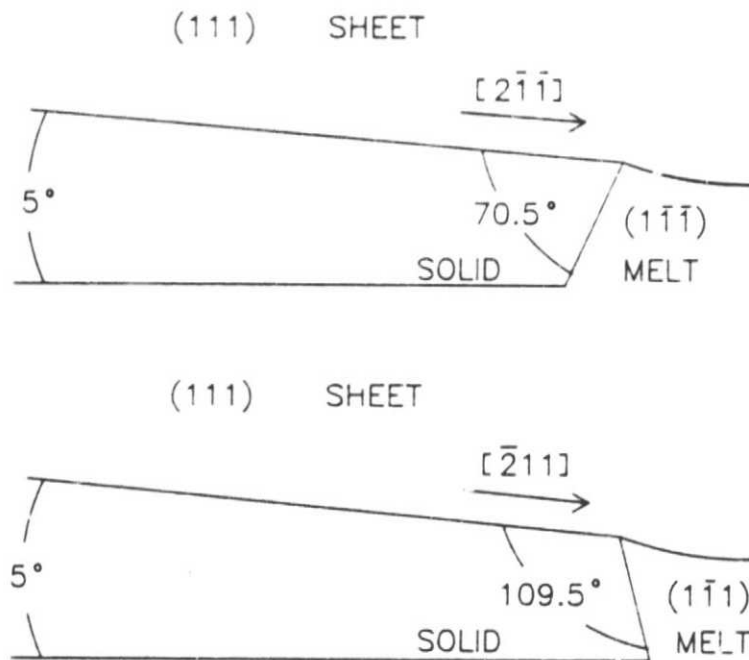
Figure 8. Predicted tip geometries for horizontally grown (111) sheets
pulled in the $\langle\bar{2}11\rangle$ and $\langle2\bar{1}\bar{1}\rangle$ directions

11
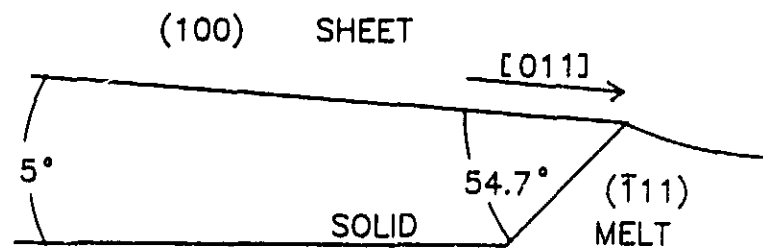
Figure 9. Predicted tip geometry for horizontal (100) sheets growing in the ⟨011⟩ directions
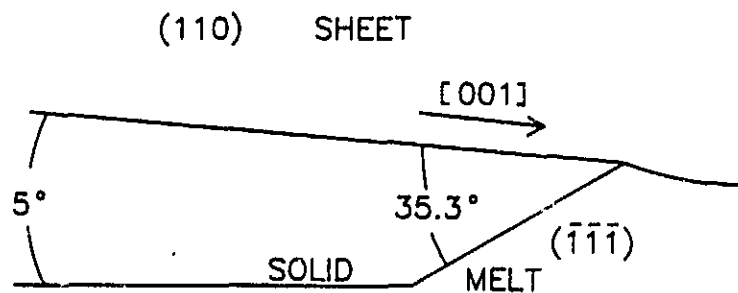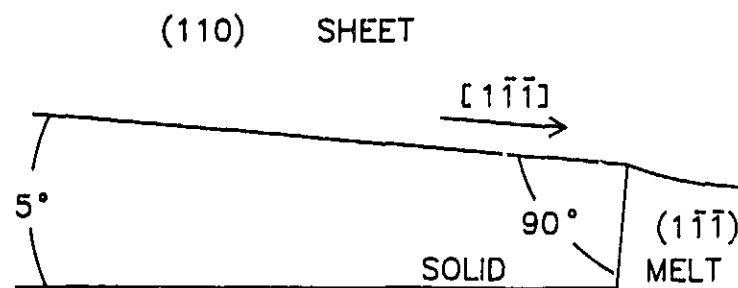
Figure 10. Predicted tip geometries for horizontal (110) sheets growing in the ⟨1I̅I̅⟩ and ⟨001⟩ directions
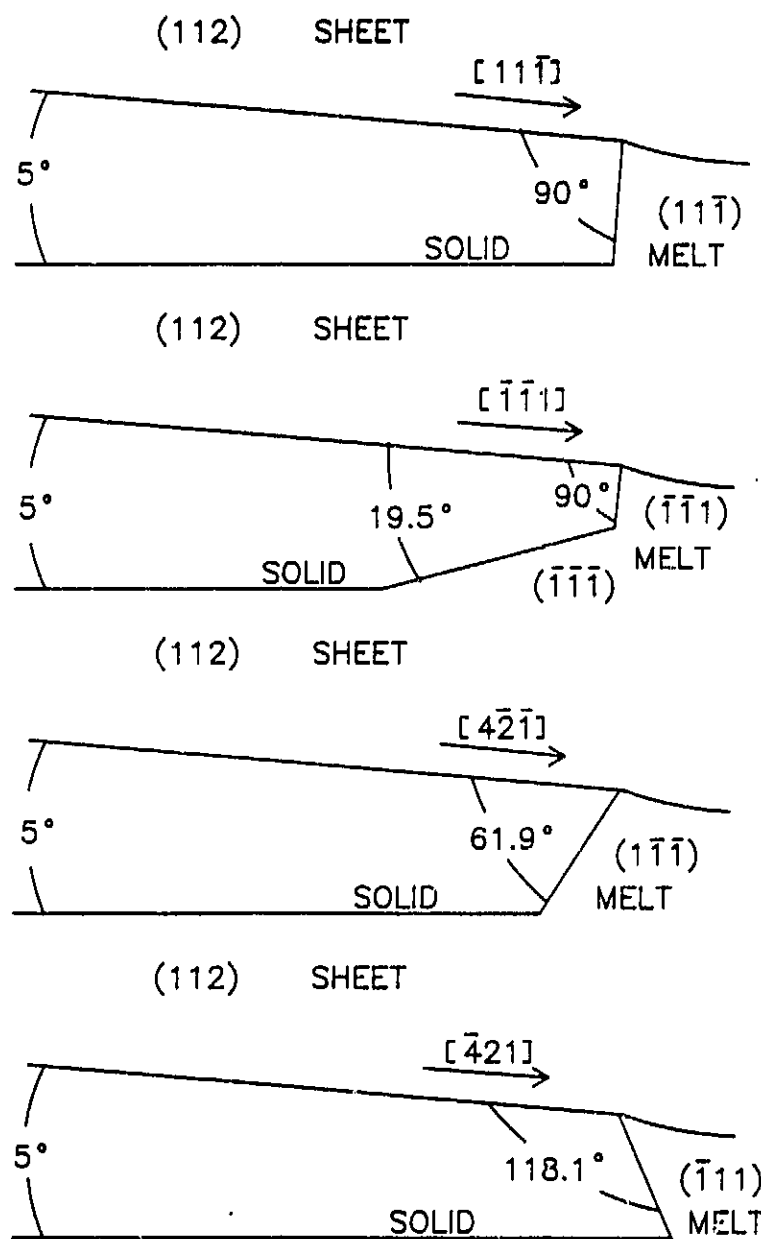
Figure 11. Predicted tip geometries for (112) sheets growing in the [11Ī], [ĪĪ1], <42Ī>, and <Ī21> directions

Figure 12. Wax-mounted (112) sheet showing a large-area $(\bar{1}\bar{1}1)$ facet on the underside meeting a $(\bar{1}\bar{1}1)$ 90° edge facet

These two facets meet at an included angle of 109.5 degrees. In the $\langle 42\bar{1}\rangle$ directions, acute angle facets of 61.9 degrees were seen, while in the $\langle \bar{4}\bar{2}1\rangle$ directions, the angles were retrograde with a 118.1-degree value.
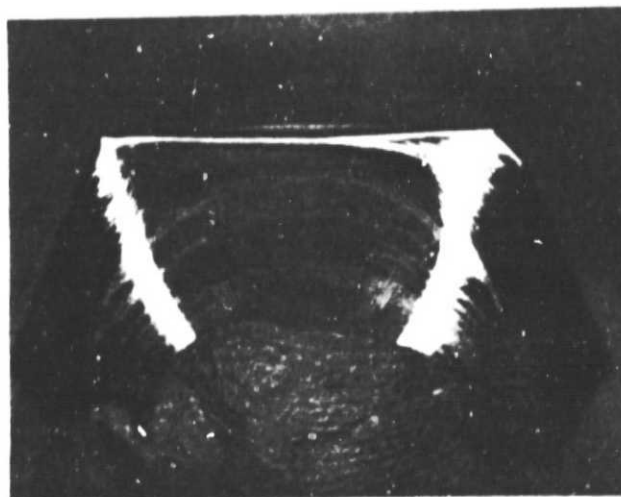
4.3 Growth Rate Anisotropies

As the radially spreading sheets described in this study evolve from the round initial geometry to the polygonal growth form, it is evident that the growth rates in the directions toward the polygon corners must be greater than the growth rates in directions toward the flat polygon sides. Neither of the rates are constant with time. Initially, the growth rate is slow, since the melt temperature does not respond immediately to the drop in RF generator power. The rate increases slowly at first, and then more rapidly, as the expanding top surface of the solid, with its higher emissivity, becomes an increasingly more effective heat radiator. The slope of a size-versus-time plot for a particular direction from the seed, at any given time, is the growth rate in that direction at that time. The ratio between rates in different directions is the ratio of slopes of the two size-versus-time curves at the same instant of time.

Figure 13 shows the size of (100) sheets along the $\langle 011\rangle$ and $\langle 001\rangle$ directions as a function of time for two different dislocation-free starting diameters, 1.2 mm and 6.2 mm. In both cases, all $\langle 011\rangle$ directions were considered to be equivalent and all $\langle 001\rangle$ directions were considered to be equivalent. Thus, four measurements for each set of directions were made for each revolution of the crystal. A second-order polynomial fit was made to the data read from the film in all cases. The small (100) sheet quickly became square
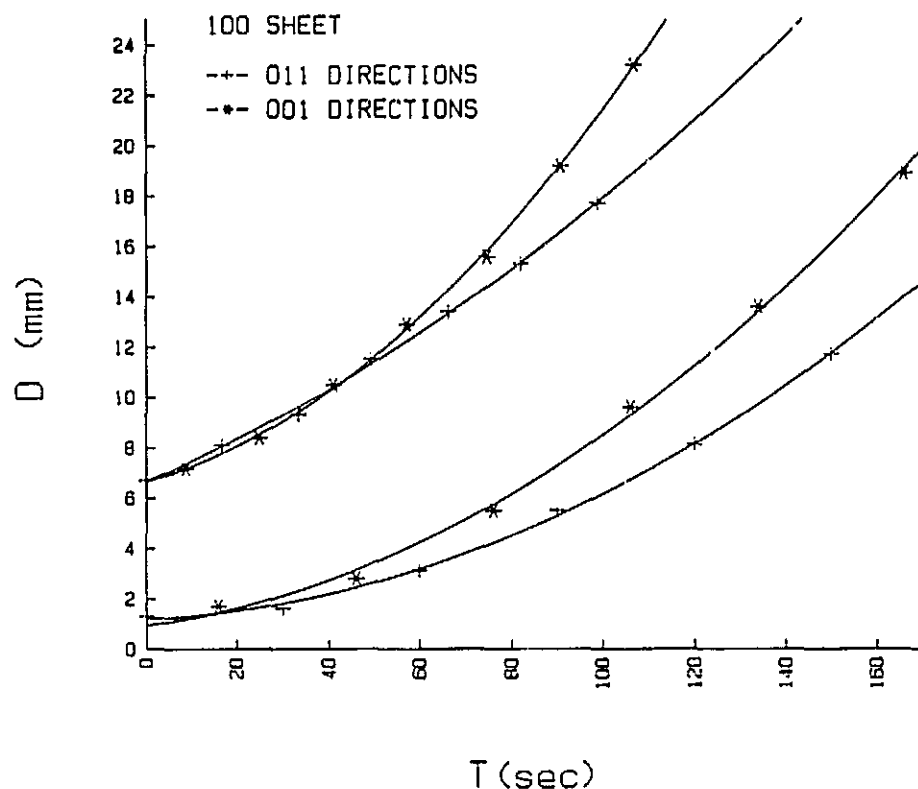
Figure 13. Size vs. time for (100) sheets of two different starting diameters

and the ratio of slopes in the ⟨011⟩ and ⟨001⟩ directions, for large times, is expected to be the geometrically limited value 0.707. The measured growth rate ratios, from the two lower curves, is 0.72. For the larger starting diameter, the sheet had not yet become square by the end of the experiment. Therefore, the rate ratio from the upper two curves is not geometrically limited, and is representative of the true growth rate anisotropy between the ⟨011⟩ and ⟨001⟩ directions. The measured ratio from the upper two curves is 0.62. A growth model for a growth rate in the ⟨011⟩ direction 0.6 times the growth rate in any other direction is shown in Figure 14. The transformation from a round to a square shape is seen to happen in about three seed diameters.

Similar behavior, but generally with less anisotropy, was seen for the other sheet planes. In all cases the growth rate in directions toward the cusps in the Wulff plots was lower than the rate in directions toward the lobes. Another example is given in Figure 15, where the size of a (110) sheet in the ⟨001⟩ and ⟨1$\bar{1}$0⟩ directions is shown as a function of time. The ⟨001⟩ growth rate is 0.83 as large as the ⟨1$\bar{1}$0⟩ growth rate. For (111) sheets, the ⟨$\bar{1}\bar{1}$2⟩ growth rate was 0.77 as large as the ⟨1$\bar{1}$0⟩ growth rate. Ratios in the vicinity of 0.8 were also seen for (112) sheets.

15
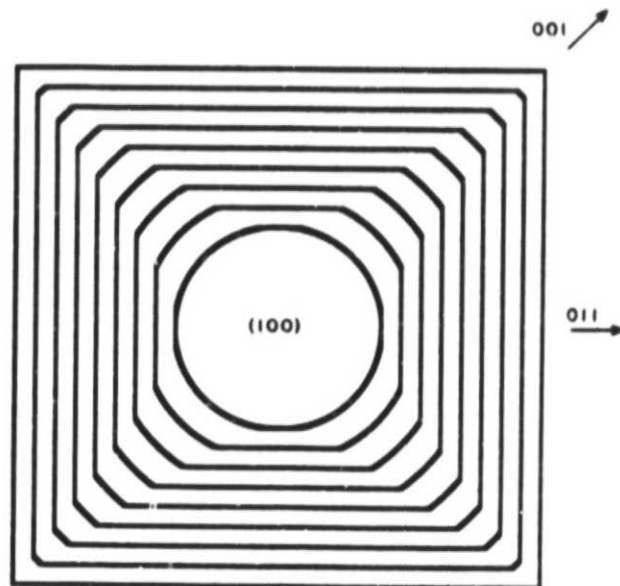
Figure 14. (100) sheet growth model for growth rate in <110> directions equal to 0.6 times the rate in all other directions
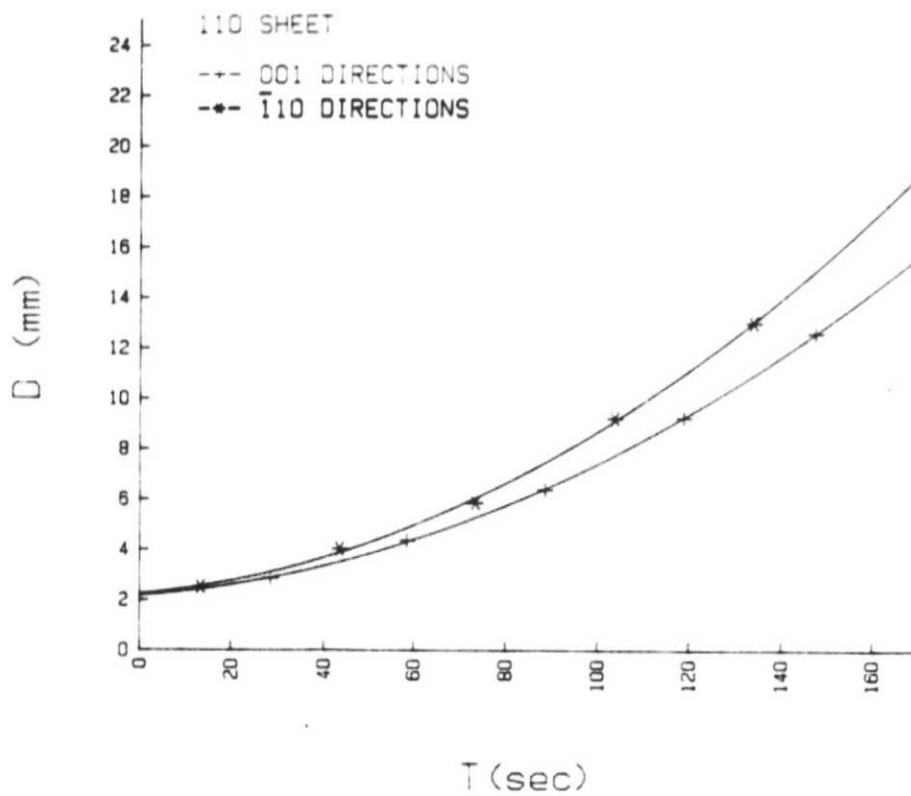

Figure 15. Size vs. time for two different growth directions in the (110) sheet plane

4.4 Polycrystalline and Dendritic Growth

Under the same conditions as those used in the dislocation-free sheet studies, some polycrystalline seeds were used to initiate sheet growth. The seeds were cut along the diameter of semiconductor-grade, chemical-vapor-deposited poly rods. At small sheet diameters, the growth was fairly uniform in all radial directions (see the left side of Figure 16). However, at larger sizes, the effects of orientation-dependent growth rates became very pronounced. This can be observed in the sheets shown in the middle and right sections of Figure 16. Especially fast-growing protrusions were dendritic in nature, like the one at the bottom right of Figure 16.

An enlarged view of a dendritic protrusion is given in the photomicrograph of Figure 17. The dendrite is single-crystalline on either side of the horizontal spine. Thus, the surface features are not crystallographic in nature but are probably growth instabilities with a constitutional supercooling origin. The dendrite does undergo a change in surface orientation at the spine region. The region above the spine has a surface plane within 2 degrees of (111), as shown by the electron channeling pattern of Figure 18a. The region below the spine has a surface plane near (115), as shown in Figure 18b. This indicates that the spine region represents the emergence of an oblique (111)-type twin plane making an angle of about 20 degrees with the dendrite surface plane.

Dendrite propagation is extremely rapid in silicon. Sixteen-millimeter films of deliberately nucleated dendrites were measured for growth rate analysis. Different dendrites propagated at different rates due to varying local conditions in the melt (proximity to other dendrites, for example). Figure 19 depicts a representative case for the increase in dendrite length and width with time. Length increases very fast at first, at rates around 2.5 m/min, and then slows as other dendrites crowd the melt and liberate heat of fusion. The width, on the other hand, increases at a rate about 25 times slower.

17
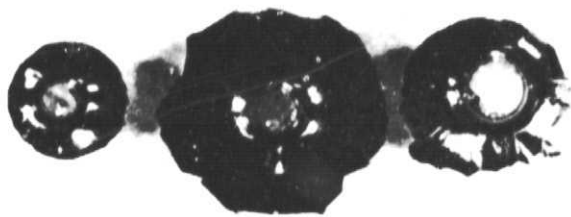
Figure 16. Three silicon sheets nucleated from a polycrystalline seed

Figure 17. Photomicrograph showing an early stage of dendritic growth from a radially expanding polycrystalline sheet. (The dendrite protrudes 1.9 mm beyond the adjacent sheet.)

18
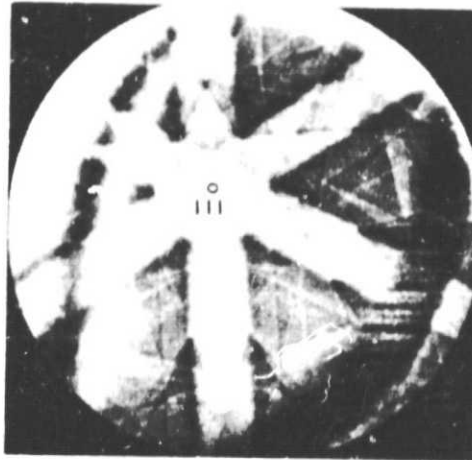
Figure 18a. Electron-channeling pattern of region above dendrite spine in
Figure 17
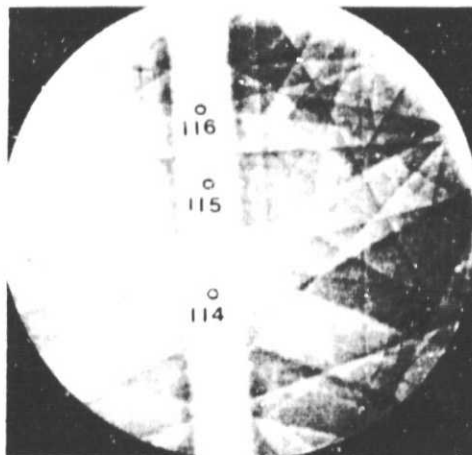
Figure 18b. Electron-channeling pattern of region below dendrite spine in
Figure 17
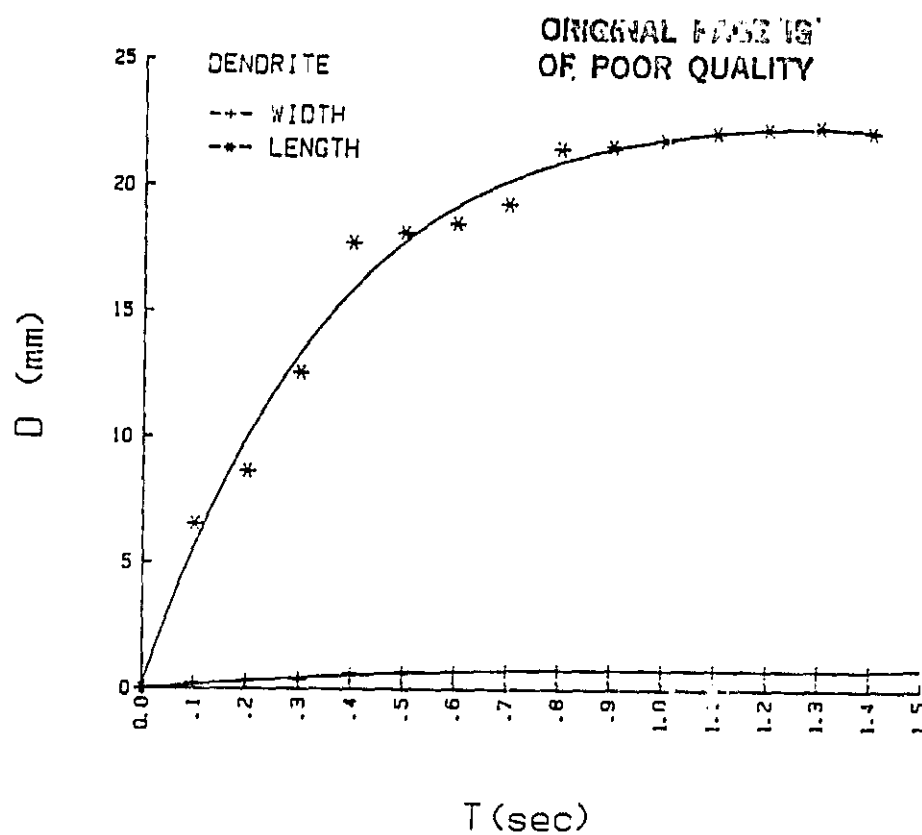
Figure 19. An example of the increase in length and width of one dendrite as a function of time

5. SUMMARY AND CONCLUSIONS

The technique of studying rapid silicon sheet growth via free spreading of point-nucleated sheets on a supercooled horizontal melt surface has yielded a large amount of information about idealized growth forms, solid/liquid interface sheet tip morphologies, qualitative Wulff surface free energy polar plots, and growth rate anisotropies. The method is versatile in that both very high perfection (dislocation-free) effects and less structured (polycrystalline and dendritic) effects can be studied.

The low surface free energy (111) planes dominate the sheet tip geometry at the solid/liquid interface, determine the growth form of radially growing sheet crystals (through their intersection with the sheet plane), and contribute to growth rate anisotropies due to the relative difficulty of new growth nucleation on the low free bond density (111) surface. They also play a determining role in fast dendritic growth by virtue of the high free bond density associated with reentrant edges at a (111) twin boundary. Earlier work on edge-supported pulling of silicon sheets [6] showed that (111) twin planes can block the spreading of spurious random grains. A similar mechanism has recently been found to be important in stabilizing the crystal structure of horizontally grown sheets. In dendritic web growth, (111) twin planes are key elements of the growth process and the (111) web surface is very high in quality. The equilibrium structure of long multicrystalline silicon sheets is dominated by longitudinal grains with (111) boundaries and near <110> surface normals. In summary, the properties of the (111) surface in silicon are of major importance for sheet crystal growth.

21

6. REFERENCES

1. Jackson, K. A., "Nucleation and Atomic Kinetics," in _Crystal Growth: A Tutorial Approach_, edited by W. Bardsley, D. T. J. Hurle, and J. B. Mullin, Amsterdam: North Holland Publishing Company, 1979.

2. Donnay, J. D. H., and D. Harker, _Am. Mineralogist_ 22, 446, 1937.

3. Jacodine, R. J., _J. Appl. Phys._, 33, 2643, 1962.

4. Wulff, G., _Z. Krist._ 34, 449, 1901.

5. Herring, C., _Phys. Rev._ 82, 87, 1951.

6. Ciszek, T. F., and J. L. Hurd, in Proc. Symp. on Electronic and Optical Properties of Polycrystalline or Impure Semiconductors and Novel Silicon Growth Methods, Pennington, NJ: The Electrochemical Society, edited by K.V. Ravi and B. O'Mara, Vol. 80-5, p. 213, 1980.

Basic Program for Generation of
Qualitative Wulff Plots and
Limiting Growth Forms

```
10 COM SP
20 PRINTER IS 1
30 CLEAR
40 DENDRITE=200
50 PRINT "THIS PROGRAM CONSTRUCTS QUALITATIVE WULFF SURFACE FREE"
60 PRINT "ENERGY POLAR PLOTS AND LIMITING GROWTH FORMS FOR SILICON"
70 PRINT "SHEET CRYSTALS WITH 100, 110, 111, 112, OR DENDRITE"
80 PRINT "SURFACE PLANES"
90 REM LANGUAGE IS HP-BASIC AND AN HP PLOTTER WITH 2 PENS IS ASSUMED
100 PRINT @ PRINT @ PPINT
110 PRINT "PREPARE THE PLOTTER AND THEN ENTER THE SURFACE PLANE"
120 INPUT SP
130 PLOTTER IS 705
140 IF SP=110 OR SP=112 THEN CHAIN "WULF112"
150 IF SP=200 THEN N=2
160 IF SP=100 THEN N=4
170 IF SP=111 THEN N=6
180 FOR J=0 TO .3 STEP .1
190 A=14+J
200 COUNT=0
210 B=A/N
220 GRAPHICS
230 GCLEAR
240 DEG
250 MOVE 83+A,50
260 WAIT 5000
270 PRINTER IS 705
280 PRINT "VS10"
290 PRINTER IS 1
300 PEN 1
310 LINE TYPE 1
320 PEN UP
330 IF N=2 THEN GOTO 450
340 FOR T=0 TO 360 STEP 1
350 X=(A+B)*COS (T)-B*COS (T*(A+B)/B)
360 Y=(A+B)*SIN (T)-B*SIN (T*(A+B)/B)
370 IF (X^2+Y^2)^.5<A+1.2*B THEN LINE TYPE 1
380 IF (X^2+Y^2)^.5>A+1.2*B THEN LINE TYPE 3
390 DRAW X+83,Y+50
400 NEXT T
410 R=A/COS (360/(2*A/B))
420 MOVE 83+A,50-R*SIN (360/(2*A/B))
430 GOTO 790
440 WAIT 10000
450 AD=30 @ BD=24+J*3
460 SCALE -20,170,0,120
470 G=4
480 MOVE AD*COS (G)+35,BD*SIN (G)+50
490 FOR C=G TO 360-G STEP 1.5
500 IF C>35 AND C<325 THEN LINE TYPE 3 ELSE LINE TYPE 1
510 XD=AD*COS (C)
520 YD=BD*SIN (C)
```

```
530 IF C<180 THEN DRAW XD+35,YD*((180-C)/180)^2+50
540 IF C>180 THEN DRAW XD+35,YD*((C-180)/180)^2+50
550 XL=XD+35
560 YLU=YD*((180-C)/180)^2+50
570 YLL=YD*((C-180)/180)^2+50
580 IF YLU<= BD*SIN (G)+50 AND COUNT=0 AND C>G THEN GOSUB 880
590 IF YLL<-(BD*SIN (G))+50 AND COUNT=1 THEN GOSUB 920
600 NEXT C
610 AD=30 @ BD=24-3*J
620 FOR C=G-180 TO 180-G STEP 1.5
630 IF C>-145 AND C<145 THEN LINE TYPE 3 ELSE LINE TYPE 1
640 XD=AD*COS (C)+60
650 YD=BD*SIN (C)
660 IF C>0 THEN GOTO 720
670 DRAW XD+35-2*(30-AD*COS (G)),YD*((-(C/180))^2)+50
680 XR=XD+35-2*(30-AD*COS (G))
690 YRL=YD*((-(C/180))^2)+50
700 IF YPL>= -(BD*SIN (G))+50 AND COUNT=2 AND C>G-180 THEN GOSUB 960
710 GOTO 760
720 DRAW XD+35-2*(30-AD*COS (G)),YD*(C/180)^2+50
730 XR=XD+35-2*(30-AD*COS (G))
740 YRU=YD*(C/180)^2+50
750 IF YPU>= BD*SIN (G)+50 AND COUNT=3 THEN GOSUB 1020
760 NEXT C
770 PEN UP
780 GOTO 830
790 PEN 2 @ WAIT 5000
800 FOR U=0 TO 360-360/(A/B) STEP 360/(A/B)
810 DRAW 83+R*COS (U+360/(2*A/B)),50+R*SIN (U+360/(2*A/B))
820 NEXT U
830 NEXT J
840 PEN 1
850 LINE TYPE 1 @ PRINTER IS 705
860 PRINT "SP0"
870 END
880 COUNT=COUNT+1
890 PEN 2
900 DXL=XL @ DYLU=YLU
910 RETURN
920 COUNT=COUNT+1
930 DYLL=YLL
940 PEN 1
950 RETURN
960 COUNT=COUNT+1
970 PEN 2
980 LINE TYPE 1
990 DRAW DXL,DYLL+.8*J
1000 DRAW XR,YRL+.8*J
1010 RETURN
1020 LINE TYPE 1
1030 DRAW DXL,DYLU+.8*J
1040 COUNT=COUNT+1
1050 DRAW XR,YRU+.8*J
1060 PEN 1
1070 RETURN
```

WULF 112

```
1100 COM SP
1110 GRAPHICS
1120 GCLEAR
1130 DEG
1140 PLOTTER IS 705
1150 SCALE -67.3,67.3,-50,50
1160 PRINTER IS 705
1170 PRINT "VS10"
1180 PRINTER IS 1
1190 FOR J=0 TO .3 STEP .1
1200 PEN 2
1210 B=14+J
1220 S1=1.26*B
1230 IF SP=110 THEN S1=.8*B
1240 A=67.7923457
1250 IF SP=110 THEN A=54.735611
1260 MOVE S1/2+B/TAN (A),0
1270 DRAW S1/2,B
1280 DRAW -(S1/2),B
1290 DRAW -(S1/2+B/TAN (A)),0
1300 DRAW -(S1/2),-B
1310 DRAW S1/2,-B
1320 DRAW S1/2+B/TAN (A),0
1330 PEN 1
1340 X1=S1/2+.5*B/TAN (A)
1350 Y1=.5*B
1360 MOVE X1,Y1
1370 A1=ATN (Y1/X1)
1380 A2=90
1390 R1=(X1^2+Y1^2)^.5
1400 R2=B
1410 GOSUB 1700
1420 A1=90
1430 A2=180-ATN (Y1/X1)
1440 R1=B
1450 R2=(X1^2+Y1^2)^.5
1460 GOSUB 1700
1470 A1=A2
1480 A2=180+ATN (Y1/X1)
1490 R1=R2
1500 R2=R1
1510 GOSUB 1700
1520 A1=A2
1530 A2=270
1540 R1=R2
1550 R2=B
1560 GOSUB 1700
1570 A1=A2
1580 A2=360-ATN (Y1/X1)
1590 R1=B
1600 R2=(X1^2+Y1^2)^.5
1610 GOSUB 1700
1620 A1=A2
```

```
1630 A2=360+ATN (Y1/X1)
1640 R1=R2
1650 R2=R1
1660 GOSUB 1700
1670 NEXT J
1680 PEN 0
1690 END
1700 FOR C=0 TO 180 STEP 4
1710 R=(R1-(R1-R2)*C/180)*(1+.4*SIN (C))
1720 T=A1+(A2-A1)*C/180
1730 X=R*COS (T)
1740 Y=R*SIN (T)
1750 IF C>35 AND C<145 THEN LINE TYPE 3 ELSE LINE TYPE 1
1760 PLOT X,Y
1770 NEXT C
1780 RETURN
```

APPENDIX B

PROGRAM PLAN

PROGRAM PLAN   AUGUST 1, 1983 - JULY 31, 1984

SOLID/MELT INTERFACE STUDIES OF
HIGH-SPEED SILICON SHEET GROWTH

TASK DESCRIPTION	AUG	SEP	OCT	NOV	DEC	JAN	FEB	MAR	APR	MAY	JUN	JUL
Investigate the influence of thermal environment upon the stability of the leading edge of silicon sheet growth from an extended solid/melt interface.	X--------O--X											
Investigate the effect of impurities on interface stability and shape.								X----------------------X				
Adapt or modify an existing ribbon growth furnace for use in support of these investigations.	X--------O-------------X											
Furnish to JPL, along with identifying data, up to 50% of the usable silicon sheet produced in the performance of this contract.								X----------------------X				